Control Engineering Practice 33 (2014) 105–114

Contents lists available at ScienceDirect

Control Engineering Practice

journal homepage: www.elsevier.com/locate/conengprac

Modified observer backstepping controller for a dynamic positioning system

H.M. Morishita *, C.E.S. Souza

University of São Paulo, Department of Naval Architecture and Ocean Engineering, São Paulo, Brazil

ARTICLE INFO

Article history:
Received 30 August 2012
Accepted 30 August 2014
Available online 14 October 2014

Keywords:
Dynamic positioning system
Observer backstepping controller
Nonlinear observer

ABSTRACT

A procedure for attenuating the control law of a vessel dynamic positioning system, based on the observer backstepping methodology, is proposed. The motivation is the appearance of an undesirable on–off behavior on the signal sent to the actuators when their saturation is considered and the control law is dependent on estimated state variables. Two gain matrices associated with the error variables are introduced to achieve the desired attenuation. Stability is proven through Lyapunov stability analysis. Numerical simulations confirm the effectiveness of the proposed controller to render the control law compatible with the limitations of the actuators.

1. Introduction

Dynamic Positioning Systems (DPS) are intended to control the horizontal motions of a vessel by exclusive means of propellers and thrusters (Fossen, 1994). Increasing operational range and performance requirements have stimulated the research community to improve on control strategies, especially to cope with challenges such as the nonlinearity of the multivariable mathematical model, stochastic perturbations, constraints on the mechanical systems (e.g., saturation of the actuators) and accurate estimation of state variables. Vessel motions are assumed to be composed of low- and wave-frequency motions. Thus, position and heading measured signals have to be filtered before they are used as an input for the controllers, since the wave-frequency component of motions is not intended to be compensated by the actuators. Early versions of DPSs adopted a notch filter to separate the low-frequency components from the total motion, while PID controllers were used to calculate the control loads assuming surge, sway and yaw motions independent from each other (Fossen, 2011). Later Balchen, Jenssen, and Saelid (1976) proposed applying a Kalman Filter (KF) to estimate the low-frequency motions of the vessel, using optimal control theory to calculate the control loads. This approach was extended and improved upon by Balchen, Jenssen, and Saelid (1980), Saelid, Jenssen, and Balchen (1983), Grimble, Patton, and Wise (1980), Fung and Grimble (1983) and Sorensen, Sagatun, and Fossen (1996). The advantage of the KF technique lies in the reduction of the phase lag induced by the filtering process (as compared to conventional low-pass or notch filters), in the possibility of implementing sensor fusion, in performing optimal estimations of the position and heading of the vessel based on sensor signals, and in the estimation of the environmental loads acting on the vessel. However, an important drawback is the need to linearize the vessel's equations of motions around a set of constant yaw angles, which imposes a time-consuming procedure for tuning of parameters and precludes assurance of global stability for the system (Fossen & Strand, 1999a; Tannuri & Pesce, 2002).

Nonlinear controllers have been considered for DPS to overcome linearization problems. Grovlen and Fossen (1996) proposed an approach with a nonlinear observer and the backstepping methodology. Fossen and Grovlen (1998) improved this idea by treating the problem in vector form, but without consideration of either filtering of wave-frequency motions or environmental loads estimation. Those works assume a stable sway–yaw dynamics condition that is removed by Robertsson and Johansson (1998). A passive nonlinear observer for both the low-frequency motions of the vessel and the environmental loads was developed by Fossen and Strand (1999a). Passivity is attained by convenient tuning of the observer gains based on a notch filter effect introduced in the mathematical model, and the observer has proven to be globally exponentially stable. Aarset, Strand, and Fossen (1998) then proposed a nonlinear controller for a DPS comprising the passive nonlinear observer and the backstepping methodology with additional integral action, but without considering the actuators dynamics. Fossen and Berge (1997) included actuator dynamics in the controller based on backstepping for tracking of marine vessels, since the bandwidths of both the actuators and vessel dynamics were close to each other. However, the controller is fed with uncorrupted position and heading signals.

An alternative nonlinear strategy for DPS was presented by Tannuri, Donha, and Pesce (2001, 2010), who proposed a controller

* Corresponding author. Tel.: +55 11 30915345; fax: +55 11 30915717.
E-mail address: hmmorish@usp.br (H.M. Morishita).

http://dx.doi.org/10.1016/j.conengprac.2014.08.012
0967-0661/

based on the Sliding Mode Control (SMC) theory. This approach showed to be robust in addressing the variations in loading and environmental conditions, as well as modeling errors. Additionally, the tuning of the SMC control parameters is simple and intuitive. However, an approach ensuring global stability for a system comprising both the controller and a state observer has yet to be presented.

Backstepping methodology involves the attainment of global stability by defining an error variable and a corresponding stabilizing function of each sub-system in association with a Lyapunov function in a systematic manner to achieve the control law. The approach also allows the introduction of additional nonlinearities into the control laws for compensation of undesirable ones (Fossen & Strand, 1999b; Khalil, 2002; Krstic, Kanellakopoulos, & Kokotovic, 1995; Marques, 2003). In DPS applications, however, the controller may induce an undesirable high-amplitude oscillatory signal. This behavior is due to the lack of a gain matrix multiplying some of the error variables that in turn may be corrupted with a parcel of wave-frequency components "leaked" from the observer estimates—an expected scenario under real situations. This aspect was observed by Zakartchouk and Morishita (2009) during the experimental evaluation of a DPS in which the controller was based on the work by Aarset et al. (1998). Preliminary analysis indicated that the reason for this behavior was the saturation of the actuators. To overcome this problem, the introduction of a gain matrix was suggested to lower the values of the deviation of the estimated positions from their desired values (an error variable) in the control loop, but no formal proof of stability was presented.

In order to achieve a more realistic DPS control law, the thrust allocation among the actuators and their saturation should be considered. Direct inclusion of such effects (specially saturation) in the control laws is a rather difficult task. In many cases, once the control law signals are defined, the thrust allocation is performed, and the saturation is subsequently imposed on the signal for each actuator. Alternatively, the thrust allocation and the corresponding saturation can be treated as an optimization problem (Johansen, Fossen, & Tondel, 2005). A proposal to consider the actuator saturation in a controller based on backstepping methodology is presented by Bateman, Hull, and Lin (2009), although neither wave-frequency motion filtering nor thrust allocation is addressed. For additional details on this subject, see Fossen (2011) and Sordalen (1997).

The main object of this paper is to propose a controller based on the observer backstepping methodology for a DPS in which both a nonlinear observer for wave-frequency motions and the actuator dynamics are included in the plant model. Besides, the controller allows a convenient tuning of the gains for the control signal to be compatible with the limitation of the actuators. In this sense, a slight modification in the controller based on observer backstepping for a DPS introduced by Aarset et al. (1998) is proposed and as a result two new gain matrices associated with error variables are included in the control structure. These matrices replace the identity gain matrices of the controller based on the conventional backstepping methodology.

The saturation of the actuators is not included in the control structure, but it is cascaded with the controller. A formulation based on a pseudo-inverse matrix is applied for dealing with the over-actuated system. The stability of the observer–controller set is proven using Lyapunov stability analysis. The assessment of the controller performance is carried out by means of dynamic simulations that consider a realistic model for the vessel dynamics and environmental loads rather than the simplified plant model considered in the design of the controller.

The text is organized as follows: Section 2 briefly presents a mathematical model of the plant for controller design purposes. In Section 3 the modified formulation for the controller based on observer backstepping is proposed. Next, stability is proven using Lyapunov stability analysis, and the rationale for the inclusion of two new gain matrices is presented. Section 4 discusses the results of the simulations, and conclusions are drawn in Section 5.

2. Mathematical model

Under assumption of small motions and considering the ship as a slender body with port/starboard symmetry, its horizontal and vertical motions may be decoupled from each other so that only the surge, sway and yaw motions—those to be controlled by the DPS—are considered in the mathematical model (Lewis, 1989; Sorensen & Strand, 2000). The vessel responses to the environmental and actuator loads are then calculated through a set of equations of motions derived in two different coordinate systems, as shown in Fig. 1. The first, *OXYZ*, is an Earth-fixed frame that can be considered as inertial for the present problem. The other frame ($GX_GY_GZ_G$) is a body-fixed one, whose axes coincide with the ship's principal axes of inertia. Both systems are assumed to be parallel to the water surface, and the direction of current, wind and waves are defined according to their orientation related to the *OX*-axis. As a DPS is exclusively intended to control low-frequency motions, only those loads due to current and the slowly varying components of wind and waves are to be considered in the models for both the controller and the observer, together with those induced by the actuators. A mathematical model suitable for the design of the controller based on observer backstepping is presented below. A more complete mathematical model for the dynamics of the vessel considered in the simulation is briefly described in Appendix A.

2.1. Low-frequency motions

The three degrees-of-freedom mathematical model for the vessel low-frequency motions consists of state-space representations of a position vector $\boldsymbol{\eta}=[X\ Y\ \psi]^T$ and a velocity vector $\boldsymbol{\nu}=[u\ v\ r]^T$, with X, Y and ψ being the coordinates for the vessel position and heading in the inertial frame and u, v, r the surge, sway and yaw velocities in the body-fixed frame respectively. For the purpose of designing the observer–controller model the environmental loads are assumed as slowly varying first-order Markov processes. The actuator dynamics are modeled through first-order differential equations. Thus, the state equations of the system are (Fossen, 1994)

$$\dot{\boldsymbol{\eta}}=\boldsymbol{J}(\boldsymbol{\eta})\boldsymbol{\nu} \tag{1}$$

$$\boldsymbol{M}\dot{\boldsymbol{\nu}}+\boldsymbol{D}\boldsymbol{\nu}=\boldsymbol{B}\boldsymbol{f}_{\boldsymbol{p}}+\boldsymbol{J}^T(\boldsymbol{\eta})\boldsymbol{b} \tag{2}$$

$$\dot{\boldsymbol{b}}=-\boldsymbol{T}_{\boldsymbol{b}}^{-1}\boldsymbol{b}+\boldsymbol{\theta}\boldsymbol{n} \tag{3}$$

$$\dot{\boldsymbol{f}}_{\boldsymbol{p}}=\boldsymbol{T}_{\boldsymbol{p}}^{-1}(\boldsymbol{f}_{\boldsymbol{d}}-\boldsymbol{f}_{\boldsymbol{p}}) \tag{4}$$

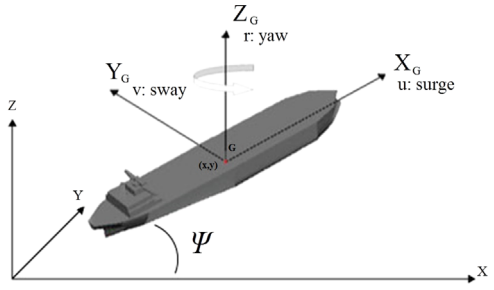

Fig. 1. Definition of the earth-fixed and body-fixed frames.

where

$$\boldsymbol{J}(\boldsymbol{\eta}) = \begin{bmatrix} \cos(\psi) & -\sin(\psi) & 0 \\ \sin(\psi) & \cos(\psi) & 0 \\ 0 & 0 & 1 \end{bmatrix} \tag{5}$$

$\boldsymbol{M} \in \mathbb{R}^{3\times3}$ is the inertia matrix including the added inertia; $\boldsymbol{D} \in \mathbb{R}^{3\times3}$ is a matrix of linear damping coefficients; $\boldsymbol{f_P} \in \mathbb{R}^m$ is the actual thrust of the m actuator vector; $\boldsymbol{B} \in \mathbb{R}^{3\times m}$ is the matrix that describes the configuration of actuators (for details see Fossen, 2011; Tannuri & Morishita, 2006); $\boldsymbol{b} \in \mathbb{R}^3$ represents the slowly-varying loads due to wind, current and second-order wave forces (related to the inertial coordinate system); $\boldsymbol{T_b} \in \mathbb{R}^{3\times3}$ is a diagonal matrix of positive time constants; $\boldsymbol{n} \in \mathbb{R}^3$ is a vector of zero-mean Gaussian white noise; $\boldsymbol{\theta} \in \mathbb{R}^{3\times3}$ is a diagonal matrix scaling the amplitude of $\boldsymbol{n}$; $\boldsymbol{T_p} \in \mathbb{R}^{m\times m}$ is a time constant diagonal matrix and $\boldsymbol{f_d} \in \mathbb{R}^m$ is the commanded thrust, i.e., the signal sent to the actuators and it is obtained from the saturation function as shown below. Let $\boldsymbol{f_c} \in \mathbb{R}^m$ be the thrust control law determined by the controller. The function that represents the saturation of the actuators can be represented as

$$\boldsymbol{f_d} = \tfrac{1}{2}\left(\boldsymbol{f_{max}} + \boldsymbol{f_{min}} - |\boldsymbol{f_{max}} - \boldsymbol{f_c}| + |\boldsymbol{f_c} - \boldsymbol{f_{min}}|\right) \tag{6}$$

where $\boldsymbol{f_{max}} \in \mathbb{R}^m$ and $\boldsymbol{f_{min}} \in \mathbb{R}^m$ are the vectors with maximum and minimum saturation values for m actuators, respectively. Notice that $\boldsymbol{f_d} = \boldsymbol{f_c}$ within the linear range of Eq. (6).

2.2. Wave-frequency motions

The wave-frequency motions of the vessel are induced essentially by the first-order wave loads and are calculated by time-domain realization of the response spectrum for each degree of freedom (see Appendix A for details). To filter out those motions from the measured position and heading signals a transfer function for each degree of freedom fed by white noise is chosen in such a way that the spectrum of its output coincides with the response spectrum of the vessel. A reasonable transfer function is

$$G_j(s) = \frac{\sigma_j s}{s^2 + 2\zeta_j \omega_{0j} s + \omega_{0j}^2}, \quad j = 1, 2, 6 \tag{7}$$

where ω_{0j}, ζ_j and σ_j are respectively the dominating wave frequency motion, the relative damping ratio, and a parameter associated with the response amplitude spectrum for each degree of freedom. j=1,2,6 denote surge, sway and yaw directions, respectively. The corresponding time domain model is given by

$$\dot{\boldsymbol{\xi}} = \boldsymbol{\Omega}\boldsymbol{\xi} + \boldsymbol{\Sigma}\boldsymbol{w_\xi} \tag{8}$$

$$\boldsymbol{\eta_{WF}} = \boldsymbol{\Gamma}\boldsymbol{\xi} \tag{9}$$

where

$$\boldsymbol{\Omega} = \begin{bmatrix} \boldsymbol{0}_{3x3} & \boldsymbol{I}_{3x3} \\ \boldsymbol{\Omega}_{21} & \boldsymbol{\Omega}_{22} \end{bmatrix}, \quad \boldsymbol{\Sigma} = \begin{bmatrix} \boldsymbol{0}_{3x3} \\ \boldsymbol{\Sigma}_2 \end{bmatrix}, \quad \boldsymbol{\Gamma} = [\boldsymbol{0}_{3x3} \;\; \boldsymbol{I}_{3x3}]$$

$$\boldsymbol{\Omega}_{21} = -diag\{\omega_{01}^2,\ \omega_{02}^2,\ \omega_{06}^2\}$$

$$\boldsymbol{\Omega}_{22} = -diag\{2\zeta_1\omega_{01},\ 2\zeta_2\omega_{02},\ 2\zeta_6\omega_{06}\}$$

$$\boldsymbol{\Sigma}_2 = diag\{\sigma_1,\ \sigma_2,\ \sigma_6\}$$

$\boldsymbol{\xi} \in \mathbb{R}^6$ is an internal variable vector and $\boldsymbol{w_\xi} \in \mathbb{R}^3$ is a vector of zero-mean Gaussian white noise.

2.3. Measurement equation

In order to complete the mathematical model it is necessary to relate the low-frequency motions, the wave-frequency amplitudes of the motions and the measurement noises of the position and heading sensors. These signals can be related through the measurement equation as

$$\boldsymbol{y} = \boldsymbol{\eta} + \boldsymbol{\eta_{WF}} + \boldsymbol{w} \tag{10}$$

where $\boldsymbol{y} \in \mathbb{R}^3$ is the measured signal vector and $\boldsymbol{w} \in \mathbb{R}^3$ is the zero-mean Gaussian white measurement noise.

3. The observer backstepping controller

The backstepping controller for a DPS requires low-frequency signals of the position and velocity, and external load vectors. As those variables are not available online an observer has to be implemented in the feedback loop, so that the controller makes use of the estimates for calculating the control law.

3.1. Nonlinear state estimator

In this work the passive nonlinear observer proposed by Fossen and Strand (1999a) is adopted. The nonlinear observer for Eqs. (1)–(3), (8)–(10) is

$$\dot{\hat{\boldsymbol{\xi}}} = \boldsymbol{\Omega}\hat{\boldsymbol{\xi}} + \boldsymbol{K}_1\tilde{\boldsymbol{y}} \tag{11}$$

$$\dot{\hat{\boldsymbol{\eta}}} = \boldsymbol{J}(\boldsymbol{y})\hat{\boldsymbol{\nu}} + \boldsymbol{K}_2\tilde{\boldsymbol{y}} \tag{12}$$

$$\dot{\hat{\boldsymbol{b}}} = -\boldsymbol{T_b}^{-1}\hat{b} + \boldsymbol{K}_3\tilde{\boldsymbol{y}} \tag{13}$$

$$\dot{\hat{\boldsymbol{\nu}}} = \boldsymbol{M}^{-1}\left[-\boldsymbol{D}\hat{\boldsymbol{\nu}} + \boldsymbol{B}\boldsymbol{f}_p + \boldsymbol{J}^T(\boldsymbol{y})\hat{b} + \boldsymbol{J}^T(\boldsymbol{y})\boldsymbol{K}_4\tilde{\boldsymbol{y}}\right] \tag{14}$$

$$\hat{\boldsymbol{y}} = \hat{\boldsymbol{\eta}} + \boldsymbol{\Gamma}\hat{\boldsymbol{\xi}} \tag{15}$$

where $\tilde{\boldsymbol{y}} = \boldsymbol{y} - \hat{\boldsymbol{y}}$ is the estimation error; $\boldsymbol{K}_1 \in \mathbb{R}^{6x3}$, $\boldsymbol{K}_2 \in \mathbb{R}^{3x3}$, $\boldsymbol{K}_3 \in \mathbb{R}^{3x3}$ and $\boldsymbol{K}_4 \in \mathbb{R}^{3x3}$ are the observer gain matrices. All assumptions and tuning procedures for assuring asymptotic convergence of the errors to zero are shown in Fossen and Strand (1999a).

3.2. Backstepping controller design

The observer backstepping controller structure is based on the work by Aarset et al. (1998), without the integral term but enhanced with the inclusion of the actuator dynamics. As it would be rather awkward to invert the saturation function (Eq. (6)) it was decided not to directly incorporate it into the controller algorithm, although it is considered in the plant model used for the simulations. Instead, the compatibility between the magnitude of the control law and the actuators capability is achieved by introducing two gain matrices associated with the error variables as shown below. A tracking function is considered in the controller structure by defining the variable $\boldsymbol{e}$ as

$$\boldsymbol{e} = \hat{\boldsymbol{\eta}} - \boldsymbol{\eta_d} \tag{16}$$

where $\boldsymbol{\eta_d}$ is a smooth reference trajectory. Time differentiation of Eq. (16) yields

$$\dot{\boldsymbol{e}} = \dot{\hat{\boldsymbol{\eta}}} - \dot{\boldsymbol{\eta}}_{\boldsymbol{d}} \tag{17}$$

The observer backstepping methodology consists of estimating $\hat{\boldsymbol{\eta}}$, $\hat{\boldsymbol{\nu}}$ and $\hat{\boldsymbol{b}}$ through Eqs. (11)–(15), while the controller is defined by taking into account three subsystems, the dynamics of which are described by Eqs. (17), (14) and (4) as shown below:

Step 1: Let an error variable $\boldsymbol{z}_1$ be defined as

$$\boldsymbol{z}_1 = \boldsymbol{e} = \hat{\boldsymbol{\eta}} - \boldsymbol{\eta_d} \tag{18}$$

Time differentiation of $\boldsymbol{z}_1$ and insertion of Eq. (12) into it results in

$$\dot{\boldsymbol{z}}_1 = \boldsymbol{J}(\boldsymbol{y})\hat{\boldsymbol{\nu}} + \boldsymbol{K}_2\tilde{\boldsymbol{y}} - \dot{\boldsymbol{\eta}}_{\boldsymbol{d}} \tag{19}$$

The term $\boldsymbol{J}(\boldsymbol{y})\hat{\boldsymbol{\nu}}$ is a good choice for virtual control of $\boldsymbol{z}_1$ dynamics.

Next, to obtain the stabilizing function $\boldsymbol{\alpha_1}$ the following Lyapunov function candidate is considered:

$$V_1 = \tfrac{1}{2}\boldsymbol{z}_1^T\boldsymbol{K_D}\boldsymbol{K_P}\boldsymbol{z}_1 \tag{20}$$

where $\boldsymbol{K_P}$ and $\boldsymbol{K_D} \in \mathbb{R}^{3x3}$ are strictly positive diagonal gain matrices. These matrices are the design control gains to be used in the next steps. Taking the time derivative of Eq. (20) along the trajectory $\boldsymbol{z}_1$, inserting Eq. (19) and substituting the virtual control with the stabilizing function yield

$$\dot{V}_1 = \boldsymbol{z}_1^T\boldsymbol{K_D}\boldsymbol{K_P}(\boldsymbol{\alpha_1} + \boldsymbol{K}_2\tilde{\boldsymbol{y}} - \dot{\boldsymbol{\eta}}_{\boldsymbol{d}}) \tag{21}$$

Next, to stabilize Eq. (19) the function $\boldsymbol{\alpha_1}$ is defined as

$$\boldsymbol{\alpha_1} = -\boldsymbol{C}_1\boldsymbol{z}_1 - \boldsymbol{D}_1\boldsymbol{z}_1 + \dot{\boldsymbol{\eta}}_{\boldsymbol{d}} \tag{22}$$

where $\boldsymbol{C}_1$ and $\boldsymbol{D}_1$ are strictly positive diagonal gain matrices. The choice for splitting the gain matrix was proposed by Fossen and Grovlen (1998) to emphasize that the first component intends to stabilize the deterministic terms of the dynamics of $\boldsymbol{z}_1$, while the latter tries to compensate the term involving the estimation error. For this purpose, and to ease the proof of stability for the observer backstepping controller, the elements of $\boldsymbol{D}_1$ are calculated based on the matrix associated with the estimation error $\tilde{y}$:

$$\boldsymbol{D}_1 = diag\left\{ d_1\boldsymbol{k}_1^T\boldsymbol{k}_1,\ d_2\boldsymbol{k}_2^T\boldsymbol{k}_2,\ d_3\boldsymbol{k}_3^T\boldsymbol{k}_3 \right\} \tag{23}$$

where $[\boldsymbol{k}_1\ \boldsymbol{k}_2\ \boldsymbol{k}_3] = \boldsymbol{K}_2^T$ and $d_i, i = 1,2,3$, are positive design constants.

Step 2: The second error variable $\boldsymbol{z}_2$ is defined as the deviation of the virtual control $\boldsymbol{J}(\boldsymbol{y})\hat{\boldsymbol{\nu}}$ from its desired value $\boldsymbol{\alpha_1}$:

$$\boldsymbol{z}_2 = \boldsymbol{J}(\boldsymbol{y})\hat{\boldsymbol{\nu}} - \boldsymbol{\alpha_1} \tag{24}$$

With this new term, the expression for $\dot{\boldsymbol{z}}_1$ becomes

$$\dot{\boldsymbol{z}}_1 = -\boldsymbol{C}_1\boldsymbol{z}_1 - \boldsymbol{D}_1\boldsymbol{z}_1 + \boldsymbol{z}_2 + \boldsymbol{K}_2\tilde{\boldsymbol{y}} \tag{25}$$

Inserting Eqs. (12), (14) and (22) into the time derivative of Eq. (24) yields (see Aarset et al., 1998 for details)

$$\dot{\boldsymbol{z}}_2 = \boldsymbol{J}(\boldsymbol{y})\boldsymbol{M}^{-1}\boldsymbol{B}\boldsymbol{f}_{\boldsymbol{p}} + \boldsymbol{\Psi} + \boldsymbol{\Omega}_1\tilde{\boldsymbol{y}} + \boldsymbol{\Omega}_2\tilde{\boldsymbol{\nu}} + \boldsymbol{\Omega}_3\tilde{\boldsymbol{\xi}} \tag{26}$$

where

$$\begin{aligned}\boldsymbol{\Psi} = {} & \boldsymbol{J}(\boldsymbol{y})\boldsymbol{S}(\hat{\boldsymbol{\rho}})\hat{\boldsymbol{\nu}} - \boldsymbol{J}(\boldsymbol{y})\boldsymbol{M}^{-1}\boldsymbol{D}\hat{\boldsymbol{\nu}} \\ & + \boldsymbol{J}(\boldsymbol{y})\boldsymbol{M}^{-1}\boldsymbol{J}^T(\boldsymbol{y})\hat{\boldsymbol{b}} - (\boldsymbol{C}_1 + \boldsymbol{D}_1)^2\boldsymbol{z}_1 \\ & + (\boldsymbol{C}_1 + \boldsymbol{D}_1)\boldsymbol{z}_2 - \ddot{\boldsymbol{\eta}}_{\boldsymbol{d}}\end{aligned} \tag{27}$$

$$\boldsymbol{\Omega}_1 = \boldsymbol{J}(\boldsymbol{y})\boldsymbol{M}^{-1}\boldsymbol{J}^T(\boldsymbol{y})\boldsymbol{K}_4 + (\boldsymbol{C}_1 + \boldsymbol{D}_1)\boldsymbol{K}_2$$

$$\boldsymbol{\Omega}_2 = -\boldsymbol{J}(\boldsymbol{y})\boldsymbol{S}(\hat{\boldsymbol{\nu}})\boldsymbol{L}; \quad \boldsymbol{\Omega}_3 = -\boldsymbol{J}(\boldsymbol{y})\boldsymbol{S}(\hat{\nu})\boldsymbol{N}$$

$$\boldsymbol{\rho} = [0\ \ 0\ \ r + \dot{\psi}_{WF}]^T$$

$\boldsymbol{S}$ is a skew-symmetrical matrix defined as

$$\boldsymbol{S}(\boldsymbol{\theta}) = \boldsymbol{S}\begin{pmatrix}\theta_1\\ \theta_2\\ \theta_3\end{pmatrix} = \begin{bmatrix}0 & -\theta_3 & \theta_2\\ \theta_3 & 0 & -\theta_1\\ -\theta_2 & \theta_1 & 0\end{bmatrix}$$

$$\boldsymbol{L} = \begin{bmatrix}0 & 0 & 0\\ 0 & 0 & 0\\ 0 & 0 & 1\end{bmatrix}; \quad \boldsymbol{N} = \begin{bmatrix}0 & 0 & 0 & 0 & 0 & 0\\ 0 & 0 & 0 & 0 & 0 & 0\\ 0 & 0 & 0 & 0 & 0 & 1\end{bmatrix}$$

$$\tilde{\boldsymbol{\nu}} = \boldsymbol{\nu} - \hat{\boldsymbol{\nu}}, \quad \tilde{\boldsymbol{\xi}} = \boldsymbol{\xi} - \hat{\boldsymbol{\xi}}$$

Eq. (26) suggests that the term $\boldsymbol{J}(\boldsymbol{y})\boldsymbol{M}^{-1}\boldsymbol{B}\boldsymbol{f}_{\boldsymbol{p}}$ is a good choice for the virtual control of $\boldsymbol{z}_2$ dynamics. An expression for its stabilizing function $\boldsymbol{\alpha_2}$ is found by defining the following Lyapunov function candidate:

$$V_2 = V_1 + \tfrac{1}{2}\boldsymbol{z}_2^T\boldsymbol{K_D}\boldsymbol{z}_2 \tag{28}$$

Time differentiation of V_2 along the trajectories $\boldsymbol{z}_1$ and $\boldsymbol{z}_2$ with the insertion of Eqs. (25) and (26) and $\boldsymbol{\alpha_2}$ results in the following equation:

$$\dot{V}_2 = \boldsymbol{z}_2^T\boldsymbol{K_D}(\boldsymbol{\alpha_2} + \boldsymbol{\Psi} + \boldsymbol{\Omega}_1\tilde{\boldsymbol{y}} + \boldsymbol{\Omega}_2\tilde{\boldsymbol{\nu}} + \boldsymbol{\Omega}_3\tilde{\boldsymbol{\xi}}) + \boldsymbol{z}_1^T\boldsymbol{K_P}\boldsymbol{z}_2 + \dot{V}_1 \tag{29}$$

Eq. (29) suggests that the stabilizing function should be defined as

$$\boldsymbol{\alpha_2} = -\boldsymbol{C}_2\boldsymbol{z}_2 - \boldsymbol{D}_2\boldsymbol{z}_2 - \boldsymbol{\Psi} - \boldsymbol{K_P}\boldsymbol{z}_1 \tag{30}$$

where $\boldsymbol{C}_2$ and $\boldsymbol{D}_2$ are strictly positive diagonal gain matrices. Again, the adoption of two matrices emphasizes the different roles of their elements. In particular, matrix $\boldsymbol{D}_2$ is calculated based on the matrices associated with estimation errors (see Eq. (26)):

$$\boldsymbol{D}_2 = diag\left\{ d_4 \sum_{i=1,4,7}\boldsymbol{\omega}_i^T\boldsymbol{\omega}_i,\ d_5 \sum_{i=2,5,8}\boldsymbol{\omega}_i^T\boldsymbol{\omega}_i,\ d_6 \sum_{i=3,6,9}\boldsymbol{\omega}_i^T\boldsymbol{\omega}_i \right\} \tag{31}$$

The vectors $\boldsymbol{\omega}_i$ are obtained as follows:

$$[\boldsymbol{\omega}_1\ \ \boldsymbol{\omega}_2\ \ \boldsymbol{\omega}_3] = \boldsymbol{\Omega}_1^T \tag{32}$$

$$[\boldsymbol{\omega}_4\ \ \boldsymbol{\omega}_5\ \ \boldsymbol{\omega}_6] = \boldsymbol{\Omega}_2^T \tag{33}$$

$$[\boldsymbol{\omega}_7\ \ \boldsymbol{\omega}_8\ \ \boldsymbol{\omega}_9] = \boldsymbol{\Omega}_3^T \tag{34}$$

$d_i,\ i = 4,5,6$, are positive constants.

Step 3: The control law is now found by introducing the actuator dynamics as modeled by Eq. (4). For this purpose a third error variable $\boldsymbol{z}_3$ is defined as the difference between the virtual control term $\boldsymbol{J}(\boldsymbol{y})\boldsymbol{M}^{-1}\boldsymbol{B}\boldsymbol{f}_{\boldsymbol{p}}$ and its desired value $\boldsymbol{\alpha_2}$, i.e.,

$$\boldsymbol{z}_3 = \boldsymbol{J}(\boldsymbol{y})\boldsymbol{M}^{-1}\boldsymbol{B}\boldsymbol{f}_{\boldsymbol{p}} - \boldsymbol{\alpha_2} \tag{35}$$

With the definition of this deviation term, $\dot{\boldsymbol{z}}_2$ can be rewritten as

$$\begin{aligned}\dot{\boldsymbol{z}}_2 = {} & -\boldsymbol{C}_2\boldsymbol{z}_2 - \boldsymbol{D}_2\boldsymbol{z}_2 + \boldsymbol{z}_3 \\ & - \boldsymbol{K_P}\boldsymbol{z}_1 + \boldsymbol{\Omega}_1\tilde{\boldsymbol{y}} + \boldsymbol{\Omega}_2\tilde{\boldsymbol{\nu}} + \boldsymbol{\Omega}_3\tilde{\boldsymbol{\xi}}\end{aligned} \tag{36}$$

Time differentiation of Eq. (35) gives

$$\dot{\boldsymbol{z}}_3 = \dot{\boldsymbol{J}}(\boldsymbol{y})\boldsymbol{M}^{-1}\boldsymbol{B}\boldsymbol{f}_{\boldsymbol{p}} + \boldsymbol{J}(\boldsymbol{y})\boldsymbol{M}^{-1}\boldsymbol{B}\dot{\boldsymbol{f}}_{\boldsymbol{p}} - \dot{\boldsymbol{\alpha}}_{\boldsymbol{2}} \tag{37}$$

The term $\dot{\boldsymbol{\alpha}}_2$ can be determined inserting Eqs. (13), (14) and (27) in the time derivative of Eq. (30). In this work, the time derivative of matrix $\boldsymbol{D}_2$ is considered as null. This assumption is reasonable since the entries of $\boldsymbol{D}_2$ are less than 1 and they are dominated by $\sin(\psi)$ and/or $\cos(\psi)$ raised to the second or fourth powers. Its time derivative can be considered null because yaw is a very slow motion (Fossen & Berge, 1997). After some mathematical work it can be expressed as

$$\begin{aligned}\dot{\boldsymbol{\alpha}}_2 = {} & \boldsymbol{\Theta}_1\boldsymbol{z}_1 + \boldsymbol{\Theta}_2\boldsymbol{z}_2 - \boldsymbol{\Theta}_3\boldsymbol{z}_3 - \left(\boldsymbol{\Psi}_0 + \boldsymbol{\Gamma}_1\boldsymbol{M}^{-1}\boldsymbol{B}\boldsymbol{f}_{\boldsymbol{p}}\right) \\ & - \boldsymbol{\Delta}_1\tilde{\boldsymbol{y}} - \boldsymbol{\Delta}_2\tilde{\boldsymbol{\nu}} - \boldsymbol{\Delta}_3\tilde{\boldsymbol{\xi}}\end{aligned} \tag{38}$$

where

$$\boldsymbol{\Theta}_1 = \boldsymbol{\Theta}_3\boldsymbol{K_P} - \left[(\boldsymbol{C}_1 + \boldsymbol{D}_1)^2 - \boldsymbol{K_P}\right](\boldsymbol{C}_1 + \boldsymbol{D}_1) \tag{39}$$

$$\boldsymbol{\Theta}_2 = \boldsymbol{\Theta}_3(\boldsymbol{C}_2 + \boldsymbol{D}_2) + (\boldsymbol{C}_1 + \boldsymbol{D}_1)^2 - \boldsymbol{K_P} \tag{40}$$

$$\boldsymbol{\Theta}_3 = (\boldsymbol{C}_1 + \boldsymbol{D}_1) + (\boldsymbol{C}_2 + \boldsymbol{D}_2) \tag{41}$$

$$\boldsymbol{\Psi}_0 = \boldsymbol{\Gamma}_1\hat{\boldsymbol{\nu}} + \boldsymbol{\Gamma}_2\boldsymbol{M}^{-1}\left[\boldsymbol{D}\hat{\boldsymbol{\nu}} + \boldsymbol{J}^T(\boldsymbol{y})\hat{\boldsymbol{b}}\right] + \boldsymbol{\Gamma}_3\hat{\boldsymbol{b}} - \ddot{\boldsymbol{\eta}}_{\boldsymbol{d}}$$

$$\boldsymbol{\Gamma}_1 = \dot{\boldsymbol{J}}(\boldsymbol{y})\left[-\boldsymbol{M}^{-1}\boldsymbol{D} + \boldsymbol{S}(\hat{\boldsymbol{\rho}})\right] + \boldsymbol{J}(\boldsymbol{y})\dot{\boldsymbol{S}}(\hat{\boldsymbol{\rho}})$$

$$\boldsymbol{\Gamma}_2 = \boldsymbol{J}(\boldsymbol{y})\left[-\boldsymbol{M}^{-1}\boldsymbol{D} + \boldsymbol{S}(\hat{\boldsymbol{\rho}})\right]$$

$$\begin{aligned}\boldsymbol{\Gamma}_3 = {} & \dot{\boldsymbol{J}}(\boldsymbol{y})\boldsymbol{M}^{-1}\boldsymbol{J}^T(\boldsymbol{y}) + \boldsymbol{J}(\boldsymbol{y})\boldsymbol{M}^{-1}\dot{\boldsymbol{J}}^T(\boldsymbol{y}) \\ & - \boldsymbol{J}(\boldsymbol{y})\boldsymbol{M}^{-1}\boldsymbol{J}^T(\boldsymbol{y})T_b^{-1}\end{aligned}$$

$$\boldsymbol{\Delta}_1 = \boldsymbol{\Theta}_3\boldsymbol{\Omega}_1 - \boldsymbol{M}^{-1}\boldsymbol{J}^T(\boldsymbol{y})\boldsymbol{K}_4 + \boldsymbol{J}(\boldsymbol{y})\boldsymbol{M}^{-1}\boldsymbol{J}^T(\boldsymbol{y})\boldsymbol{K}_3$$

$$-\left[(\boldsymbol{C}_1+\boldsymbol{D}_1)^2-\boldsymbol{K_P}\right]\boldsymbol{K}_2$$

$$\boldsymbol{\Delta}_2=\boldsymbol{\Theta}_3\boldsymbol{\Omega}_2;\quad \boldsymbol{\Delta}_3=\boldsymbol{\Theta}_3\boldsymbol{\Omega}_3$$

The terms $\boldsymbol{\Gamma}_1$ and $\boldsymbol{\Gamma}_3$ require $\dot{\boldsymbol{J}}(\boldsymbol{y})$. To calculate this value, the following assumptions are adopted: (a) $\boldsymbol{y}(3)=\psi+\psi_{WF}+\boldsymbol{d}(3)\approx\psi$ because the magnitude of the wave-induced heading (ψ_{WF}) is less than 1° during normal operation of the vessel and the measurement noise $\boldsymbol{d}(3)$ is negligible compared to ψ_{WF}; (b) the low-frequency yaw motion estimate obtained from the observer is taken into account. This approach is quite reasonable because the yaw motion is adequately estimated by the observer from the measured signal (see Fossen & Strand, 1999a for details of above assumptions). Thus $\dot{\boldsymbol{J}}(\boldsymbol{y})=\boldsymbol{J}(\boldsymbol{y})\boldsymbol{S}([0\ 0\ \hat{\nu}(3)]^T)$. Inserting Eq. (38) into Eq. (37) and taking into account Eq. (4) with $\boldsymbol{f_d}=\boldsymbol{f_c}$ result in

$$\begin{aligned}\dot{\boldsymbol{z}}_3=&\boldsymbol{\Theta}_4\boldsymbol{f_c}+(\boldsymbol{\Theta}_5-\boldsymbol{\Theta}_4)\boldsymbol{f_p}-\boldsymbol{\Theta}_1\boldsymbol{z}_1-\boldsymbol{\Theta}_2\boldsymbol{z}_2\\&+\boldsymbol{\Theta}_3\boldsymbol{z}_3+\dot{\boldsymbol{\Psi}}_0+\boldsymbol{\Delta}_1\tilde{\boldsymbol{y}}+\boldsymbol{\Delta}_2\tilde{\boldsymbol{\nu}}+\boldsymbol{\Delta}_3\tilde{\boldsymbol{\xi}}\end{aligned}\tag{42}$$

where

$$\boldsymbol{\Theta}_4=\boldsymbol{J}(\boldsymbol{y})\boldsymbol{M}^{-1}\boldsymbol{B}\boldsymbol{T}_p^{-1}$$

$$\boldsymbol{\Theta}_5=\dot{\boldsymbol{J}}(\boldsymbol{y})\boldsymbol{M}^{-1}\boldsymbol{B}+\boldsymbol{\Gamma}_2\boldsymbol{M}^{-1}\boldsymbol{B}\tag{43}$$

Next, in an attempt to find the control law $\boldsymbol{f_c}$ the following Lyapunov function candidate can be defined:

$$V_3=V_2+\tfrac{1}{2}\boldsymbol{z}_3^T\boldsymbol{z}_3\tag{44}$$

Taking the time differentiation of Eq. (44) along the trajectories $\boldsymbol{z}_1$, $\boldsymbol{z}_2$ and $\boldsymbol{z}_3$ and considering Eqs. (25), (36), (42) yield

$$\begin{aligned}\dot{V}_3=&\boldsymbol{z}_3^T[\boldsymbol{\Theta}_4\boldsymbol{f_c}+(\boldsymbol{\Theta}_5-\boldsymbol{\Theta}_4)\boldsymbol{f_p}-\boldsymbol{\Theta}_1\boldsymbol{z}_1\\&+(\boldsymbol{K_D}-\boldsymbol{\Theta}_2\boldsymbol{z}_2+\boldsymbol{\Theta}_3\boldsymbol{z}_3+\dot{\boldsymbol{\Psi}}_0\\&+\boldsymbol{\Delta}_1\tilde{\boldsymbol{y}}+\boldsymbol{\Delta}_2\tilde{\boldsymbol{\nu}}+\boldsymbol{\Delta}_3\tilde{\boldsymbol{\xi}}]+\dot{V}_2\end{aligned}\tag{45}$$

Finally, Eq. (45) suggests that the control law can be calculated as

$$\begin{aligned}\boldsymbol{f_c}=&(\boldsymbol{I}-\boldsymbol{\Theta}_4^+\boldsymbol{\Theta}_5)\boldsymbol{f_p}+\boldsymbol{\Theta}_4^+[\boldsymbol{\Theta}_1\boldsymbol{z}_1+(\boldsymbol{\Theta}_2-\boldsymbol{K_D})\boldsymbol{z}_2\\&-(\boldsymbol{C}_3\boldsymbol{D}_3+\boldsymbol{\Theta}_3)\boldsymbol{z}_3-\dot{\boldsymbol{\Psi}}_0]\end{aligned}\tag{46}$$

$$\boldsymbol{\Theta}_4^+=\boldsymbol{\Theta}_4^T(\boldsymbol{\Theta}_4\boldsymbol{\Theta}_4^T)^{-1}\tag{47}$$

where $\boldsymbol{\Theta}_4^+$ is the pseudo-inverse of $\boldsymbol{\Theta}_4$ used to cope with the over-actuated system (Fossen, 1994), and $\boldsymbol{C}_3$ and $\boldsymbol{D}_3$ are diagonal positive definite matrices. The latter is defined in a similar manner as for $\boldsymbol{D}_2$, i.e.,

$$\begin{aligned}\boldsymbol{D}_3=diag\Bigg\{&d_7\sum_{i=10,13,16}\boldsymbol{\omega}_i^T\boldsymbol{\omega}_i,\\&d_8\sum_{i=11,14,17}\boldsymbol{\omega}_i^T\boldsymbol{\omega}_i,\ d_9\sum_{i=12,15,18}\boldsymbol{\omega}_i^T\boldsymbol{\omega}_i\Bigg\}\end{aligned}\tag{48}$$

where the vectors $\boldsymbol{\omega}_i$ are defined as

$$[\boldsymbol{\omega}_{10}\ \boldsymbol{\omega}_{11}\ \boldsymbol{\omega}_{12}]=\boldsymbol{\Delta}_1^T\tag{49}$$

$$[\boldsymbol{\omega}_{13}\ \boldsymbol{\omega}_{14}\ \boldsymbol{\omega}_{15}]=\boldsymbol{\Delta}_2^T\tag{50}$$

$$[\boldsymbol{\omega}_{15}\ \boldsymbol{\omega}_{16}\ \boldsymbol{\omega}_{17}]=\boldsymbol{\Delta}_3^T\tag{51}$$

Inserting Eq. (46) into Eq. (42) yields the last error dynamics, i.e.,

$$\dot{\boldsymbol{z}}_3=-\boldsymbol{C}_3\boldsymbol{z}_3-\boldsymbol{D}_3\boldsymbol{z}_3-\boldsymbol{K_D}\boldsymbol{z}_2+\boldsymbol{\Delta}_1\tilde{\boldsymbol{y}}+\boldsymbol{\Delta}_2\tilde{\boldsymbol{\nu}}+\boldsymbol{\Delta}_3\tilde{\boldsymbol{\xi}}\tag{52}$$

In principle, the observer and the controller (see Eqs. (14) and (46)) require $\boldsymbol{f_p}$, that is, the real thrust developed by the actuators. These values are very difficult to be measured online for utilization in the controller. Alternatively, the thrust calculated from Eq. (4) is assumed as the real thrust of the actuators.

3.3. Stability analysis for the observer backstepping controller

3.3.1. Error dynamics and equilibrium point

The stability analysis of the closed-loop system with observer backstepping controller is carried out through the assessment of the error dynamics equations for both the controller and the observer. These equations can be expressed concisely by defining $\boldsymbol{z}=[\boldsymbol{z}_1^T\ \boldsymbol{z}_2^T\ \boldsymbol{z}_3^T]^T$ and taking into account Eqs. (11)–(15), (25), (36) and (52):

$$\dot{\boldsymbol{z}}=-\boldsymbol{C}_z\boldsymbol{z}-\boldsymbol{D}_z\boldsymbol{z}+\boldsymbol{E}\boldsymbol{z}+\boldsymbol{W}_1\tilde{\boldsymbol{y}}+\boldsymbol{W}_2\tilde{\boldsymbol{\nu}}+\boldsymbol{W}_3\tilde{\boldsymbol{\xi}}\tag{53}$$

$$\dot{\tilde{\boldsymbol{\nu}}}=\boldsymbol{M}^{-1}\left[-\boldsymbol{D}\tilde{\boldsymbol{\nu}}-\boldsymbol{J}^T(y)\tilde{\boldsymbol{z}}_0\right]\tag{54}$$

$$\dot{\tilde{\boldsymbol{x}}}_0=\boldsymbol{A}_0\tilde{\boldsymbol{x}}_0+\boldsymbol{B}_0\boldsymbol{J}(\boldsymbol{y})\tilde{\boldsymbol{\nu}}\tag{55}$$

$$\tilde{\boldsymbol{z}}_0=\boldsymbol{C}_0\tilde{\boldsymbol{x}}_0\tag{56}$$

where $\tilde{\boldsymbol{x}}_0=\left[\tilde{\boldsymbol{\xi}}^T\ \tilde{\boldsymbol{\eta}}^T\ \tilde{\boldsymbol{b}}^T\right]^T$; $\tilde{\boldsymbol{b}}=\boldsymbol{b}-\hat{\boldsymbol{b}}$

$$\boldsymbol{C}_z=diag\{\boldsymbol{C}_1,\ \boldsymbol{C}_2,\ \boldsymbol{C}_3\}\tag{57}$$

$$\boldsymbol{D}_z=diag\{\boldsymbol{D}_1,\ \boldsymbol{D}_2,\ \boldsymbol{D}_3\}\tag{58}$$

$$\boldsymbol{E}=\begin{bmatrix}\boldsymbol{0}&\boldsymbol{I}&\boldsymbol{0}\\-\boldsymbol{K_P}&\boldsymbol{0}&\boldsymbol{I}\\\boldsymbol{0}&-\boldsymbol{K_D}&\boldsymbol{0}\end{bmatrix}\tag{59}$$

$$\boldsymbol{W}_1=\left[\boldsymbol{K}_2^T\ \boldsymbol{\Omega}_1^T\ \boldsymbol{\Delta}_1^T\right]^T\tag{60}$$

$$\boldsymbol{W}_2=\left[\boldsymbol{0}\ \boldsymbol{\Omega}_2^T\ \boldsymbol{\Delta}_2^T\right]^T\tag{61}$$

$$\boldsymbol{W_3}=\left[\boldsymbol{0}_{3x6}^T\ \boldsymbol{\Omega}_3^T\ \boldsymbol{\Delta}_3^T\right]^T\tag{62}$$

$$\boldsymbol{A}_0=\begin{bmatrix}\boldsymbol{\Omega}-\boldsymbol{K}_1\boldsymbol{\Gamma}&-\boldsymbol{K}_1&\boldsymbol{0}\\-\boldsymbol{K}_2\boldsymbol{\Gamma}&-\boldsymbol{K}_2&\boldsymbol{0}\\-\boldsymbol{K}_3\boldsymbol{\Gamma}&-\boldsymbol{K}_3&-\boldsymbol{T}_{\boldsymbol{b}}^{-1}\end{bmatrix}$$

$$\boldsymbol{B}_0=[\boldsymbol{0}\ \boldsymbol{I}\ \boldsymbol{0}]^T;\ \boldsymbol{C}_0=[\boldsymbol{K}_4\boldsymbol{\Gamma}\ \boldsymbol{K}_4\ -\boldsymbol{I}]$$

From Eqs. (53)–(55) it immediately comes that the origin $[\boldsymbol{z}^T\ \tilde{\boldsymbol{\nu}}^T\ \tilde{\boldsymbol{x}}_0^T]^T=\boldsymbol{0}_{24x1}$ is an equilibrium point for the closed-loop observer backstepping system.

3.3.2. Stability analysis

For the proof of the stability two key assumptions adopted by Fossen and Strand (1999a) are pointed out here:

A.1 $\boldsymbol{M}=\boldsymbol{M}^T>\boldsymbol{0}$;
A.2 $(\boldsymbol{D}+\boldsymbol{D}^T)>\boldsymbol{0}$.

A Lyapunov function candidate that copes with both the observer and the controller error dynamics is

$$V=\tfrac{1}{2}\boldsymbol{z}^T\boldsymbol{R}\boldsymbol{z}+\tilde{\boldsymbol{\nu}}^T\boldsymbol{M}\tilde{\boldsymbol{\nu}}+\tilde{\boldsymbol{x}}_0^T\boldsymbol{P}\tilde{\boldsymbol{x}}_0\tag{63}$$

where

$$\boldsymbol{R}=\begin{bmatrix}\boldsymbol{K_P}\boldsymbol{K_D}&\boldsymbol{0}&\boldsymbol{0}\\\boldsymbol{0}&\boldsymbol{K_D}&\boldsymbol{0}\\\boldsymbol{0}&\boldsymbol{0}&\boldsymbol{I}\end{bmatrix}\tag{64}$$

$$\boldsymbol{P}\in\mathbb{R}^{12x12},\quad \boldsymbol{P}=\boldsymbol{P}^T>\boldsymbol{0}$$

Next, taking the time derivative of V along trajectories of $\boldsymbol{z}$, $\tilde{\boldsymbol{\nu}}$ and $\tilde{\boldsymbol{x}}_0$ results in:

$$\dot{V}=\boldsymbol{z}^T(-\boldsymbol{R}\boldsymbol{C}_z\boldsymbol{z}-\boldsymbol{R}\boldsymbol{D}_z\boldsymbol{z}+\boldsymbol{R}\boldsymbol{W}_1\tilde{\boldsymbol{y}}+\boldsymbol{R}\boldsymbol{W}_2\tilde{\boldsymbol{\nu}}$$

$$+\boldsymbol{R}W_3\tilde{\boldsymbol{\xi}})-\tilde{\boldsymbol{\nu}}^T\boldsymbol{Q}_1\tilde{\boldsymbol{\nu}}-\tilde{\boldsymbol{x}}_0^T\boldsymbol{Q}_2\tilde{\boldsymbol{x}}_0 \tag{65}$$

where

$$\boldsymbol{D}^T+\boldsymbol{D}=\boldsymbol{Q}_1>\boldsymbol{0}$$

$$\boldsymbol{P}\boldsymbol{A}_0+\boldsymbol{A}_0^T\boldsymbol{P}=-\boldsymbol{Q}_2<\boldsymbol{0}$$

Note that $\boldsymbol{z}^T\boldsymbol{R}\boldsymbol{E}\boldsymbol{z}=\boldsymbol{0}$ because $\boldsymbol{R}\boldsymbol{E}$ is skew-symmetric. From Eq. (65) it is not easy to immediately establish a conclusion concerning the sign of $\dot{V}$ because there are no obvious square terms. The following terms are then added to $\dot{V}$:

$$\tfrac{1}{4}[\tilde{\boldsymbol{y}}^T\boldsymbol{G}_1\tilde{\boldsymbol{y}}-\tilde{\boldsymbol{y}}^T\boldsymbol{G}_1\tilde{\boldsymbol{y}}]=\boldsymbol{0} \tag{66}$$

$$\tfrac{1}{4}[\tilde{\boldsymbol{\nu}}^T\boldsymbol{G}_2\tilde{\boldsymbol{\nu}}-\tilde{\boldsymbol{\nu}}^T\boldsymbol{G}_2\tilde{\boldsymbol{\nu}}]=\boldsymbol{0} \tag{67}$$

$$\tfrac{1}{4}[\tilde{\boldsymbol{\xi}}^T\boldsymbol{G}_3\tilde{\boldsymbol{\xi}}-\tilde{\boldsymbol{\xi}}^T\boldsymbol{G}_3\tilde{\boldsymbol{\xi}}]=\boldsymbol{0} \tag{68}$$

where

$$\boldsymbol{G}_i=g_i\boldsymbol{I},\quad i=1,2,3 \tag{69}$$

$$g_1=\frac{1}{4}\sum_{i=1}^{3}\left[\frac{\boldsymbol{K_D}(i,i)\boldsymbol{K_P}(i,i)}{d_i}+\frac{\boldsymbol{K_D}(i,i)}{d_{i+3}}+\frac{1}{d_{i+6}}\right]$$

$$g_2=g_3=\frac{1}{4}\sum_{i=1}^{3}\left[\frac{1}{d_{i+3}}+\frac{\boldsymbol{K_D}^{-1}(i,i)}{d_{i+6}}\right]$$

Then, inserting Eqs. (66)–(68) into Eq. (65) and relating $\tilde{\boldsymbol{y}}$ and $\tilde{\boldsymbol{\xi}}$ to $\tilde{\boldsymbol{x}}_0$ as $\tilde{\boldsymbol{y}}=\boldsymbol{C}_y\tilde{\boldsymbol{x}}_0$ and $\tilde{\boldsymbol{\xi}}=\boldsymbol{C}_\xi\tilde{\boldsymbol{x}}_0$ it becomes

$$\begin{aligned}\dot{V}=&-\boldsymbol{z}^T\boldsymbol{R}\boldsymbol{C}_z\boldsymbol{z}+\boldsymbol{z}^T\left(-\boldsymbol{R}\boldsymbol{D}_z\boldsymbol{z}+\boldsymbol{R}\boldsymbol{W}_1\tilde{\boldsymbol{y}}+\boldsymbol{R}\boldsymbol{W}_2\tilde{\boldsymbol{\nu}}+\boldsymbol{R}\boldsymbol{W}_3\tilde{\boldsymbol{\xi}}\right)\\&-\tfrac{1}{4}\left(\tilde{\boldsymbol{y}}^T\boldsymbol{G}_1\tilde{\boldsymbol{y}}+\tilde{\boldsymbol{\nu}}^T\boldsymbol{G}_2\tilde{\boldsymbol{\nu}}+\tilde{\boldsymbol{\xi}}^T\boldsymbol{G}_3\tilde{\boldsymbol{\xi}}\right)\\&-\tilde{\boldsymbol{x}}_0^T\left(\boldsymbol{Q}_2-\tfrac{1}{4}\boldsymbol{C}_y^T\boldsymbol{G}_1\boldsymbol{C}_y-\tfrac{1}{4}\boldsymbol{C}_\xi^T\boldsymbol{G}_3\boldsymbol{C}_\xi\right)\tilde{\boldsymbol{x}}_0\\&-\tilde{\boldsymbol{\nu}}^T(\boldsymbol{Q}_1-\tfrac{1}{4}\boldsymbol{G}_2)\tilde{\boldsymbol{\nu}}\end{aligned} \tag{70}$$

In Eq. (70) the matrix $\boldsymbol{R}\boldsymbol{C}_z$ is positive definite and the addition of the second and third terms results in a negative semidefinite function, namely:

$$\begin{aligned}\lambda=&\boldsymbol{z}^T\left(-\boldsymbol{R}\boldsymbol{D}_z\boldsymbol{z}+\boldsymbol{R}\boldsymbol{W}_1\tilde{\boldsymbol{y}}+\boldsymbol{R}\boldsymbol{W}_2\tilde{\boldsymbol{\nu}}+\boldsymbol{R}\boldsymbol{W}_3\tilde{\boldsymbol{\xi}}\right)\\&-\tfrac{1}{4}\left(\tilde{\boldsymbol{y}}^T\boldsymbol{G}_1\tilde{\boldsymbol{y}}+\tilde{\boldsymbol{\nu}}^T\boldsymbol{G}_2\tilde{\boldsymbol{\nu}}+\tilde{\boldsymbol{\xi}}^T\boldsymbol{G}_3\tilde{\boldsymbol{\xi}}\right)\le 0\end{aligned} \tag{71}$$

as proven in Appendix B. Now, if the matrices $\boldsymbol{Q}_1$ and $\boldsymbol{Q}_2$ are chosen as

$$\boldsymbol{Q}_1-\tfrac{1}{4}\boldsymbol{G}_2>0 \tag{72}$$

$$\left(\boldsymbol{Q}_2-\tfrac{1}{4}\boldsymbol{C}_y^T\boldsymbol{G}_1\boldsymbol{C}_y-\tfrac{1}{4}\boldsymbol{C}_\xi^T\boldsymbol{G}_3\boldsymbol{C}_\xi\right)>\boldsymbol{0} \tag{73}$$

it can be concluded that

$$\begin{aligned}\dot{V}\le&-\boldsymbol{z}^T\boldsymbol{R}\boldsymbol{C}_z\boldsymbol{z}\\&-\tilde{\boldsymbol{x}}_0^T\left(\boldsymbol{Q}_2-\tfrac{1}{4}\boldsymbol{C}_y^T\boldsymbol{G}_1\boldsymbol{C}_y-\tfrac{1}{4}\boldsymbol{C}_\xi^T\boldsymbol{G}_3\boldsymbol{C}_\xi\right)\tilde{\boldsymbol{x}}_0\\&-\tilde{\boldsymbol{\nu}}^T(\boldsymbol{Q}_1-\tfrac{1}{4}\boldsymbol{G}_2)\tilde{\boldsymbol{\nu}}<0,\quad\forall\ \boldsymbol{z},\tilde{\boldsymbol{\nu}},\tilde{\boldsymbol{x}}_0\neq\boldsymbol{0}\end{aligned} \tag{74}$$

Hence, the observer backstepping system (Eqs. (53)–(55)) is Globally Exponentially Stable (GES) if assumptions A.1 and A.2 hold and if the matrices $\boldsymbol{Q}_1$ and $\boldsymbol{Q}_2$ satisfy Eqs. (72) and (73) (Fossen, 2011; Khalil, 2002). Notice that the controller based on observer backstepping methodology assures stability by assuming an unrestricted magnitude for the control law.

3.4. System constraints and the role of matrices $\boldsymbol{K_P}$ and $\boldsymbol{K_D}$

In general, dynamic positioning systems are not designed to counteract all possible combinations of external forces and moment, and their actuators have limited power. The first practical consequence is that the stability of the closed-loop system is restricted to a basin of attraction for a given origin. The determination of this basin demands an intense numerical task that is beyond the purpose of this paper. The second possible consequence is an occasional incompatibility between the magnitude of the control law defined by Eq. (46) and the capability of the actuators. In this equation, matrices $\boldsymbol{\Theta}_4^+$ and $\boldsymbol{\Theta}_5$ cannot be tuned since they depend essentially on the plant parameters (see Eqs. (47) and (43)). Furthermore, the former matrix works as a gain for all terms inside the bracket. The remaining parameters associated with the error variables, namely $\boldsymbol{\theta}_1$, $\boldsymbol{\theta}_2-\boldsymbol{K_D}$ and $\boldsymbol{C}_3+\boldsymbol{D}_3+\boldsymbol{\theta}_3$, are the design control parameters (see Eqs. (39), (40) and (41)). Now, let us suppose that the entries of matrix $\boldsymbol{\Theta}_4^+$ are such that the design control parameters have absolute values much smaller than 1, so that the magnitude of the control law is compatible with the limitation of actuators. Recalling that all matrices are diagonal, these conditions can be expressed as

Condition 1

$$\begin{aligned}|\boldsymbol{\Theta}_1(i,i)|=&|[\boldsymbol{CD}_1(i,i)+\boldsymbol{CD}_2(i,i)]\boldsymbol{K_P}(i,i)\\&-[\boldsymbol{CD}_1^2(i,i)-\boldsymbol{K_P}(i,i)]\boldsymbol{CD}_1(i,i)|\ll 1\end{aligned} \tag{75}$$

Condition 2

$$\begin{aligned}|\boldsymbol{\Theta}_2(i,i)-\boldsymbol{K_D}(i,i)|=&|[\boldsymbol{CD}_1(i,i)+\boldsymbol{CD}_2(i,i)]\boldsymbol{CD}_2(i,i)\\&+\boldsymbol{CD}_1^2(i,i)-\boldsymbol{K_P}(i,i)-\boldsymbol{K_D}(i,i)|\ll 1\end{aligned} \tag{76}$$

Condition 3

$$\begin{aligned}0<\boldsymbol{CD}_3(i,i)+\boldsymbol{\Theta}_3(i,i)=&\boldsymbol{CD}_1(i,i)+\boldsymbol{CD}_2(i,i)\\&+\boldsymbol{CD}_3(i,i)\ll 1\end{aligned} \tag{77}$$

where $\boldsymbol{CD}_i=\boldsymbol{C}_i+\boldsymbol{D}_i$ for $i=1,2,3$ Condition 3 imposes that all entries in matrices $\boldsymbol{C}_i$ and $\boldsymbol{D}_i$ must be much smaller than 1. It is useful to analyze the consequences of this condition for the controller based on the conventional backstepping methodology in which $\boldsymbol{K_P}=\boldsymbol{K_D}=\boldsymbol{I}$. In this case Condition 2 is immediately invalidated because $[\boldsymbol{CD}_1(i,i)+\boldsymbol{CD}_2(i,i)]\boldsymbol{CD}_2(i,i)+[\boldsymbol{CD}_1(i,i)]^2\approx 2$ cannot be satisfied. Besides, $\boldsymbol{\theta}_1\approx 2\boldsymbol{CD}_1(i,i)+\boldsymbol{CD}_2(i,i)-[\boldsymbol{CD}_1(i,i)]^2$ can at times fail to satisfy Condition 1. Therefore, the controller based on the conventional backstepping methodology may lead to an incompatibility between the control parameters for some control specifications. This drawback can, however, be overcome by inserting the matrices $\boldsymbol{K_P}$ and $\boldsymbol{K_D}$ proposed in this paper.

4. Simulation results and discussion

The controller performance is evaluated here through numerical simulations of low-speed maneuvres with a typical DP-shuttle tanker equipped with five actuators—one main propeller, two bow thrusters and two stern thrusters. The vessel main dimensions and the actuator properties are shown in Tables 1 and 2, respectively. A realistic model was adopted for representing the vessel dynamics (Appendix A). The values for matrices $\boldsymbol{M}$, $\boldsymbol{B}$ and $\boldsymbol{T_p}$ are indicated in Appendix C, together with the environmental conditions adopted in the simulations.

Smooth variation of the references for position, velocity and acceleration is required by the controller. These signals are generated by applying a step change to the following fourth-order transfer function:

$$H(s)=\frac{1}{(25s+1)^2}\frac{0.02^2}{(s^2+0.0404s+0.02^2)} \tag{78}$$

The transfer function of Eq. (78) is employed for each degree of freedom of the vessel, and the amplitude of the step function corresponds to the vessel's final desired position. The simulation begins with the initial setpoint vector [0 m, 0 m, 0°] constant for 100 s, and then the ship is demanded to move to [20 m, −10 m, 15°],

Table 1
Vessel particulars.

Total length (m)	272.5
Length between perp. (m)	258.0
Beam (m)	46.0
Draft (m)	17.5
Total displacement (kN)	178.0×10^7

Table 2
Actuator thrust ranges and positions.

Actuators	Maximum thrust	Position (from CG)
Main propeller	1200 kN/−550 kN	−129.0 m
Stern thruster 1	180 kN/−180 kN	−125.0 m
Stern thruster 2	180 kN/−180 kN	−120.0 m
Bow thruster 1	260 kN/−260 kN	120.0 m
Bow thruster 2	260 kN/−260 kN	125.0 m

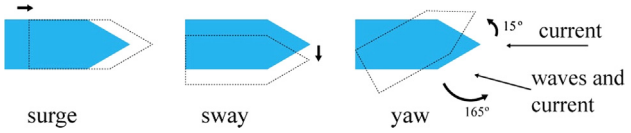

Fig. 2. Maneuvres for simulations.

Table 3
Control parameters.

$\boldsymbol{C}_1$	$diag\{0.02,\ 0.02,\ 0.02\}$
$\boldsymbol{C}_2$	$diag\{10^{-5},\ 10^{-5},\ 10^{-5}\}$
$\boldsymbol{C}_3$	$diag\{10^{-3},\ 10^{-3},\ 10^{-3}\}$
$d_i\ i=1,2,3$	$d_1=0.2,\ d_2=0.2,\ d_3=0.2$
$d_i\ i=4,5,6$	$d_4=0.02;\ d_5=0.01;\ d_6=0.002$
$d_i\ i=7,8,9$	$d_7=0.1;\ d_8=0.01;\ d_9=0.01$

Table 4
Coefficients of vectors $\boldsymbol{z}_1$, $\boldsymbol{z}_2$ and $\boldsymbol{z}_3$ for $\boldsymbol{K_P}=\boldsymbol{K_D}=\boldsymbol{I}$.

$\boldsymbol{\Theta}_1$	$diag\{0.273,\ 0.250,\ 0.250\}$
$\boldsymbol{\Theta}_2-\boldsymbol{K_D}$	$diag\{-1.980;\ -1.984,\ -1.984\}$
$\boldsymbol{C}_3+\boldsymbol{D}_3+\boldsymbol{\Theta}_3$	$diag\{0.199,\ 0.132,\ 0.132\}$

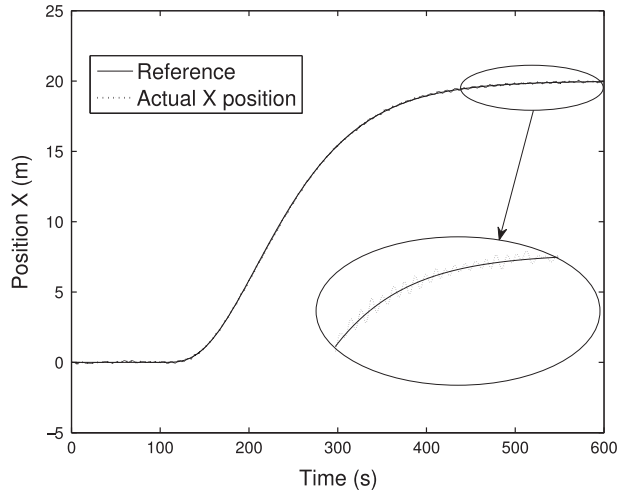

Fig. 3. Position of the vessel along X-axis—the zoom displays the difference between the reference and actual position.

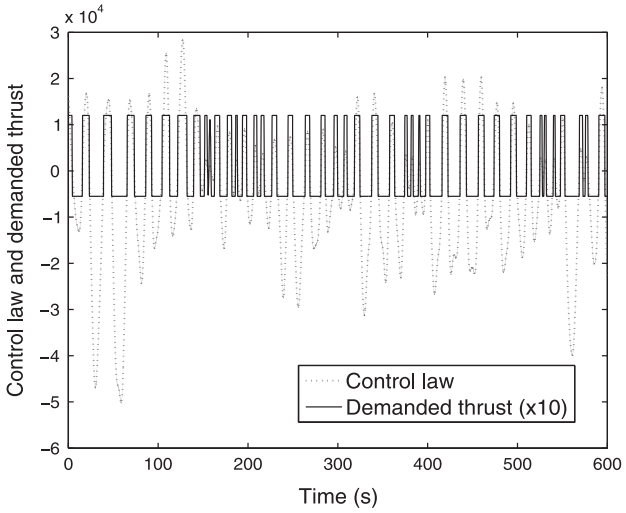

Fig. 4. Control law and commanded thrust for the main propeller.

as indicated in Fig. 2. Notice that these maneuvres check the performance of the observer and the controller simultaneously for set point changes and for the alteration in the relative environmental loads due to the change in the vessel heading.

The combination of the vessel's parameters indicated in Appendix C with heading angle $\psi=0$ results in the order of magnitude of some elements of $\boldsymbol{\Theta}_4^+ \sim 10^{11}$. Also, numerical analyses have shown that $\boldsymbol{z}_1 \sim 10^{-1}$, $\boldsymbol{z}_2 \sim 10^{-1}$ and $\boldsymbol{z}_3 \sim 10^{-2}$, leading to $\boldsymbol{f_P} \sim 10^7$ kN, which is not compatible with the actuators capacity as indicated in Table 2. Thus, the use of the controller based on the modified observer backstepping algorithm is adequate. However, it is worthwhile initially to analyze the performance of the controller based on conventional backstepping methodology by tuning $\boldsymbol{K_P}=\boldsymbol{K_D}=\boldsymbol{I}$, while cascading the saturation function of the actuators. The values for matrix $\boldsymbol{C}$ and for coefficients d_i are shown in Table 3, and the corresponding coefficients associated with vectors $\boldsymbol{z}_1$, $\boldsymbol{z}_2$ and $\boldsymbol{z}_3$ are indicated in Table 4. Notice that the entries of matrices $\boldsymbol{\Theta}_1$ and $\boldsymbol{\Theta}_2-\boldsymbol{K_D}$ do not comply with Conditions 1 and 2.

Fig. 3 shows the reference $\boldsymbol{\eta_d}(1)$ and the vessel motion in the X direction. It may be said that the proposed observer backstepping controller operates properly in both the steady-state and the transient conditions since the curves are in acceptable agreement along all of their extents. However, the inappropriate tuning of the control parameters leads to awkward behavior for both the control law and the commanded thrust as depicted in Fig. 4. It should be remarked that the plotted values of the commanded thrust are multiplied by 10. The on–off-like signal (Astrom & Hagglund, 1995) is caused by the oscillatory control signal that periodically exceeds the saturation values of the actuators. The outline of the control law is due to the combination of inappropriate control parameters and the unavoidable oscillation of the estimated values $\hat{\boldsymbol{\eta}}$, $\hat{\boldsymbol{\nu}}$ and $\hat{\boldsymbol{b}}$ that are sensitive to the estimation error and therefore affect error variables—recall that the measured signal is corrupted with wave-frequency motions. The results for the Y direction and the heading present similar patterns to those depicted in Figs. 3 and 4 and are thus omitted.

Now, the gain matrices $\boldsymbol{K_P}=diag\{0.01,\ 0.01,\ 0.01\}$ and $\boldsymbol{K_D}=diag\{0.002,\ 0.002,\ 0.002\}$ are considered together with the design control parameters indicated in Table 3, leading to the coefficients associated with the variable errors shown in Table 5 that indicate compliance with Conditions 1–3. The evolution of the ship position and heading is shown in Fig. 5. The control law operates as expected because the vessel follows a smooth reference trajectory during the transient and steady-state conditions.

Table 5
Coefficients of vectors z_1, z_2 and z_3 for $K_P \neq I, K_D \neq I$.

Θ_1	$diag\{0.135,\ 0.526,\ 0.525\}10^{-3}$
$\Theta_2 - K_D$	$diag\{0.71,\ 0.39,\ 0.39\}10^{-3}$
Θ_3	$diag\{0.138,\ 0.126,\ 0.126\}$

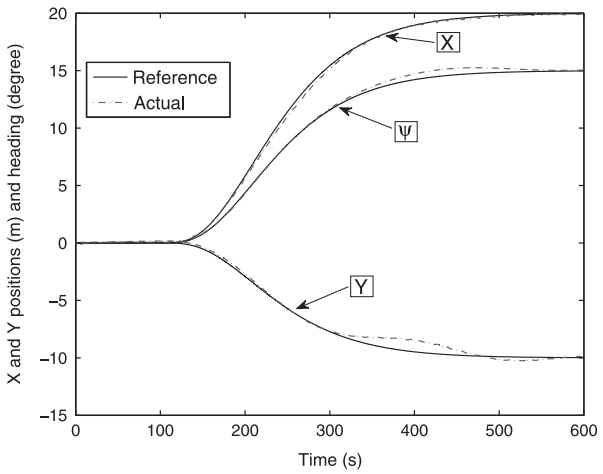

Fig. 5. Position and heading of the vessel.

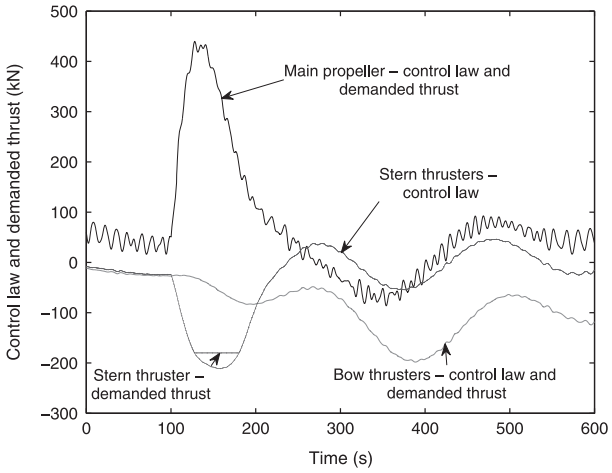

Fig. 6. Control law and commanded thrust for each actuator.

The most important results, however, are those shown in Fig. 6, which depicts the control law and the commanded thrust. Comparison with Fig. 4 reveals a dramatic difference as the unsuitable oscillation for both curves is no longer present. In fact, some oscillation still persists due to the position and heading estimation errors, but with magnitude of approximately 10^1 kN in steady-state condition, which can be deemed acceptable for practical purposes. Regarding the transient condition, Fig. 6 reveals that the stern thrusters become saturated, but not enough to cause either loss of stability or oscillation in the control law. It is important to recall here that the main goal of the proposed approach is not to eliminate occasional needs for the actuators to operate in the saturated range, but rather to reduce the oscillatory behavior of the control law provoked by the estimation error in association with the saturation of the actuators. Therefore, the presented results indicate the effectiveness of inserting the new gain matrices K_P and K_D in the control loop, within the context of the backstepping methodology.

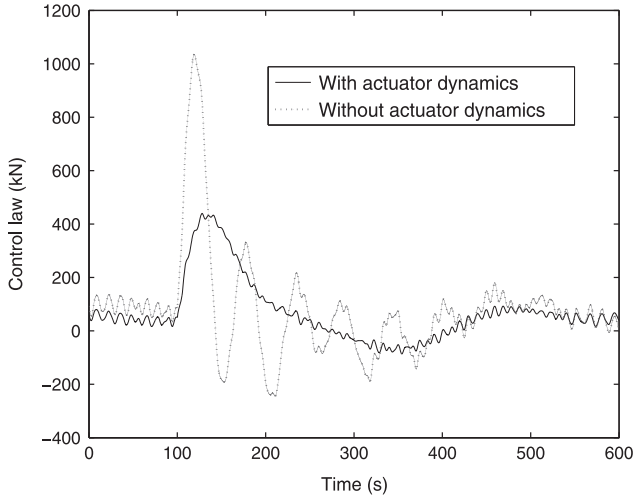

Fig. 7. Control laws for surge with and without inclusion of the actuator dynamics.

This subsection is concluded by demonstrating the advantage of including the actuator dynamics in the control loop. For this purpose, the performance of the proposed controller and that of an observer backstepping controller without the inclusion of the actuator dynamics are compared. The latter is based on Eq. (30) and only the gain matrix K_P is available to lower the control signal magnitude (see Zakartchouk & Morishita, 2009). By considering the actuator dynamics as an inherent part of the plant model, the same maneuvres shown previously were considered here, and the results for the surge motion (which is assumed to be typical) are depicted in Fig. 7. This figure reveals that it is worthwhile to implement the controller with actuator dynamics because the control signals are less demanding and smoother than those defined by the controller without the actuator dynamics. The time lag between the control law and the real thrust caused by the actuator dynamics tends to retard the vessel motions, and the controller without inclusion of actuator dynamics tends to compensate for it by magnifying its output. This is an expected result since the proposed controller is based on a more accurate plant model that includes the actuator dynamics, whose bandwidth is close to the bandwidth of the vessel dynamics.

5. Conclusions

Controllers based on conventional observer backstepping for DPS may generate a control signal incompatible with the actuators capability, when the error variables corrupted with remnant wave-frequency signals due to non-perfect state estimation are amplified by control gains exclusively determined by the system parameters. The proposed improvement consists in inserting two new gain matrices associated with the error variables, in order to attenuate the oscillations in the control signal. Numerical simulations with a realistic plant model confirm the efficacy of the solution here introduced, as the undesirable on–off-like control signals vanish when the proposed modification is included. In addition, the simulation results also indicate the advantage of including the actuator dynamics in the control law as the signal is smoothed even in the absence of the wave-frequency motions. However, the inclusion of the actuator dynamics in the control algorithm requires the tuning of a time constant set for first-order differential equations. Occasional mismatch between the "real time constant" and the controller time constant does not affect the stability of the closed-loop control system, but can degrade the performance of the controller. Therefore, for a practical scenario, a

preliminary study to estimate the real time lag of the actuators is suggested before tuning the controller time constant.

Stability of the closed-loop system with the improved controller is assured through Lyapunov stability analysis. Global exponential stability is attained if saturation of the actuators is ignored; otherwise, exponential stability is obtained for some region of attraction.

The implementation of the new controller is simple and some criteria that define the range of appropriate values of the new control parameters were presented. However, the augmentation of the control parameters may be considered as a drawback, since it demands the tuning of new parameters. An optimization approach could be considered in future works, instead of the trial and error procedure adopted here. Another desirable improvement would be the inclusion of the actuators limitation in the control law itself. This, however, is not a simple task because of the difficulty in inverting the saturation equation. The proposed observer backstepping controller was developed for a specific mechanical system, viz. a dynamic positioning system for a vessel. However, the methodology can be useful for any system in which the filtering of undesirable high-frequency motion components is based on a state estimator, and where power limitation of the actuators is an issue.

Appendix A. Mathematical model for the dynamic simulation

A.1. Low-frequency motions

The low-frequency motions model for the vessel is composed of Eq. (1) and the following kinematic equation:

$$\begin{aligned}&\boldsymbol{M}\dot{\boldsymbol{\nu}}+[\boldsymbol{C}_{\boldsymbol{RB}}(\boldsymbol{\nu})+\boldsymbol{C}_{\boldsymbol{A}}(\boldsymbol{\nu})]\boldsymbol{\nu}-\boldsymbol{M}_{\boldsymbol{A}}\dot{\boldsymbol{\nu}}_{\boldsymbol{c}}\\&\quad+\boldsymbol{C}_{\boldsymbol{A}}(\boldsymbol{\nu})\boldsymbol{\nu}_{\boldsymbol{c}}-\boldsymbol{C}_{\boldsymbol{A}}(\boldsymbol{\nu}_{\boldsymbol{c}})\boldsymbol{\nu}_{\boldsymbol{r}}\\&\quad=\boldsymbol{B}\boldsymbol{f}_{\boldsymbol{P}}+\boldsymbol{f}_{\boldsymbol{e}}\end{aligned}\tag{A.1}$$

where

$$\boldsymbol{\nu}_{\boldsymbol{r}}=\boldsymbol{\nu}-\boldsymbol{\nu}_{\boldsymbol{c}}$$

$$\boldsymbol{\nu}_{\boldsymbol{c}}=[U\ \cos(\psi_c-\psi)\ \ U\ \sin(\psi_c-\psi)\ \ 0]^T$$

$$\boldsymbol{f}_{\boldsymbol{e}}=[F_X\ F_Y\ N]^T$$

M_A is the added mass matrix of the vessel; C_{RB} is the rigid-body Coriolis and centripetal matrix; C_A is the hydrodynamic Coriolis and centripetal matrix; U is the current speed; ψ_c is the direction of the current with respect to the OX-axis; F_X, F_Y and N represent the total external forces and moment in the surge, sway and yaw directions, respectively. The entries of the vector $\boldsymbol{f}_{\boldsymbol{e}}$ are forces and moment due to the action of the current, wind and waves. In this work the forces and moment due to the current are determined through the model proposed by Simos, Tannuri, Pesce, and Aranha (2001). The wind forces and moment are calculated employing aerodynamic drag equations with coefficients presented in OCIMF (1994). See Fossen (1994) for alternative models. The wind forces and moment are determined considering the relative wind speed and its relative angle of incidence on the vessel. The low-frequency motions due to the waves are caused by the so-called slow and mean-drift forces (Aranha, 1996; Aranha & Fernandes, 1995).

Wave-frequency motions: The wave-frequency motions of the vessel are in essence due to the first-order wave loads and can be included in the simulation mathematical model by generating a time series from the wave frequency amplitude spectrum. The spectrum for each degree of freedom is given by (Fossen, 2011)

$$S_{WF}(\omega,\psi_{rw})=|RAO(\omega,\psi_{rw})|^2S(\omega,T_0,H_s)\tag{A.2}$$

$$\psi_{rw}=\psi-\psi_w$$

where RAO is the ship Response Amplitude Operator which is the transfer function that represents the response of the vessel to an incident regular wave of unit amplitude, and ψ_w is the wave direction related to the OX-axis. The RAO should be calculated for a set of wave directions, and then the vector $\boldsymbol{\eta}_{WF}\in\mathbb{R}^3$ with the amplitude of the wave-frequency motions can be generated from the spectrum defined by Eq. (A.2) (Fossen, 1994).

Appendix B. Proof of Eq. (71)

The proof is based on Fossen and Grovlen (1998). Recalling Eqs. (58), (60)–(62) and (64), Eq. (71) can be rewritten as

$$\begin{aligned}\lambda=&\boldsymbol{z}_1^T(-\boldsymbol{K}_{\boldsymbol{D}}\boldsymbol{K}_{\boldsymbol{P}}\boldsymbol{D}_1\boldsymbol{z}_1+\boldsymbol{K}_{\boldsymbol{D}}\boldsymbol{K}_{\boldsymbol{P}}\boldsymbol{K}_2\tilde{\boldsymbol{y}})\\&+\boldsymbol{z}_2^T(-\boldsymbol{K}_{\boldsymbol{D}}\boldsymbol{D}_2\boldsymbol{z}_2+\boldsymbol{K}_{\boldsymbol{D}}\boldsymbol{\Omega}_1\tilde{\boldsymbol{y}}+\boldsymbol{K}_{\boldsymbol{D}}\boldsymbol{\Omega}_2\tilde{\boldsymbol{\nu}}+\boldsymbol{K}_{\boldsymbol{D}}\boldsymbol{\Omega}_3\tilde{\boldsymbol{\xi}})\\&+\boldsymbol{z}_3^T(-\boldsymbol{D}_3\boldsymbol{z}_3+\boldsymbol{\Delta}_1\tilde{\boldsymbol{y}}+\boldsymbol{\Delta}_2\tilde{\boldsymbol{\nu}}+\boldsymbol{\Delta}_3\tilde{\boldsymbol{\xi}})\\&-\tfrac{1}{4}(\tilde{\boldsymbol{y}}^T\boldsymbol{G}_1\tilde{\boldsymbol{y}}+\tilde{\boldsymbol{\nu}}^T\boldsymbol{G}_2\tilde{\boldsymbol{\nu}}+\tilde{\boldsymbol{\xi}}^T\boldsymbol{G}_3\tilde{\boldsymbol{\xi}})\end{aligned}\tag{B.1}$$

Now, considering Eqs. (23), (31), (32)–(34), (48) and (49)–(51) in (B.1) yields

$$\begin{aligned}\lambda=-\sum_{i=1}^{3}\Bigg[&d_i\boldsymbol{K}_{\boldsymbol{P}}(i,i)\boldsymbol{K}_{\boldsymbol{D}}(i,i)\left(\boldsymbol{k}_i\boldsymbol{z}_1(i)-\frac{1}{2d_i}\tilde{\boldsymbol{y}}\right)^T\left(\boldsymbol{k}_i\boldsymbol{z}_1(i)-\frac{1}{2d_i}\tilde{\boldsymbol{y}}\right)\\&+d_{i+3}\boldsymbol{K}_{\boldsymbol{D}}(i,i)\left(\boldsymbol{\omega}_i\boldsymbol{z}_2(i)-\frac{1}{2d_{i+3}}\tilde{\boldsymbol{y}}\right)^T\left(\boldsymbol{\omega}_i\boldsymbol{z}_2(i)-\frac{1}{2d_{i+3}}\tilde{\boldsymbol{y}}\right)\\&+d_{i+3}\boldsymbol{K}_{\boldsymbol{D}}(i,i)\left(\boldsymbol{\omega}_{i+3}\boldsymbol{z}_2(i)-\frac{1}{2d_{i+3}}\tilde{\boldsymbol{\nu}}\right)^T\left(\boldsymbol{\omega}_{i+3}\boldsymbol{z}_2(i)-\frac{1}{2d_{i+3}}\tilde{\boldsymbol{\nu}}\right)\\&+d_{i+3}\boldsymbol{K}_{\boldsymbol{D}}(i,i)\left(\boldsymbol{\omega}_{i+6}\boldsymbol{z}_2(i)-\frac{1}{2d_{i+3}}\tilde{\boldsymbol{\xi}}\right)^T\left(\boldsymbol{\omega}_{i+6}\boldsymbol{z}_2(i)-\frac{1}{2d_{i+3}}\tilde{\boldsymbol{\xi}}\right)\\&+d_{i+6}\left(\boldsymbol{\omega}_{i+9}\boldsymbol{z}_3(i)-\frac{1}{2d_{i+6}}\tilde{\boldsymbol{y}}\right)^T\left(\boldsymbol{\omega}_{i+9}\boldsymbol{z}_3(i)-\frac{1}{2d_{i+6}}\tilde{\boldsymbol{y}}\right)\\&+d_{i+6}\left(\boldsymbol{\omega}_{i+12}\boldsymbol{z}_3(i)-\frac{1}{2d_{i+6}}\tilde{\boldsymbol{\nu}}\right)^T\left(\boldsymbol{\omega}_{i+12}\boldsymbol{z}_3(i)-\frac{1}{2d_{i+6}}\tilde{\boldsymbol{\nu}}\right)\\&+d_{i+6}\left(\boldsymbol{\omega}_{i+15}\boldsymbol{z}_3(i)-\frac{1}{2d_{i+6}}\tilde{\boldsymbol{\xi}}\right)^T\left(\boldsymbol{\omega}_{i+15}\boldsymbol{z}_3(i)-\frac{1}{2d_{i+6}}\tilde{\boldsymbol{\xi}}\right)\Bigg]\end{aligned}\tag{B.2}$$

where $[\boldsymbol{z}_i(1)\ \boldsymbol{z}_i(2)\ \boldsymbol{z}_i(3)]^T=\boldsymbol{z}_i$ for $i=1,2,3$

Because all quadratic terms in Eq. (B.2) are less than or equal to zero, Eq. (71) is negative semidefinite.

Appendix C. Simulation data

The following data were used in this paper:

$$\boldsymbol{M}_{\boldsymbol{RB}}=diag\{1.74\times10^8,\ 1.74\times10^8,\ 1.08\times10^{12}\}$$

$$\boldsymbol{M}_{\boldsymbol{A}}=\begin{bmatrix}1.1\times10^7&0&0\\0&1.5\times10^8&3.8\times10^7\\0&3.7\times10^7&5.4\times10^7\end{bmatrix}$$

$$\boldsymbol{T}_{\boldsymbol{p}}=diag\{10s,\ 5s,\ 5s\}$$

$$\boldsymbol{B}=\begin{bmatrix}1&0&0&0&0\\0&1&1&1&1\\0&-125&-120&120&125\end{bmatrix}$$

$$\boldsymbol{K}_{\boldsymbol{1}}=\begin{bmatrix}-1.98&0&0\\0&-1.98&0\\0&0&-1.98\\1.26&0&0\\0&1.19&0\\0&0&-1.19\end{bmatrix}$$

$\boldsymbol{K_2} = diag\{0.768,\ 0.728,\ 0.828\}$

$\boldsymbol{K_3} = diag\{10^{-4},\ 10^{-4},\ 1\}10^{9}$

$\boldsymbol{K_4} = 100\boldsymbol{K_3}$

$\boldsymbol{T_b} = diag\{1000,\ 1000,\ 1000\}$

Environmental data

	Direction	Velocity
Current	180°	0.5 m/s
Wind	165°	10.0 m/s
Waves	165°	$T_p = 9$ s; $H_s = 2.5$ m

References

Aarset, M. F., Strand, J. P., & Fossen, T. I. (1998). Nonlinear vectorial observer backstepping with integral action and wave filtering for ships. In *Proceedings of the IFAC conference on control applications in marine systems* (*CAMS*'98), *Fukuoka, Japan* (pp. 83–89).

Aranha, J. A. P. (1996). Second-order horizontal steady forces and moment on a floating body with small forward speed. *Journal of Fluid Mechanics*, *303*, 39–54.

Aranha, J. A. P., & Fernandes, A. C. (1995). On the second-order slow drift force spectrum. *Applied Ocean Research*, *17*(5), 311–313.

Astrom, K., & Hagglund, T. (1995). *PID controllers: Theory, design, and tuning* (2nd ed.). Research Triangle Park, NC: Instrument Society of America.

Balchen, J. G., Jenssen, N. A., & Saelid, S. (1976). Dynamic positioning using Kalman filtering and optimal control theory. In *IFAC/IFIP symposium on automation in offshore oil field operation* (pp. 183–186).

Balchen, J. G., Jenssen, N. A., & Saelid, S. (1980). Dynamic positioning of floating vessels based on Kalman filtering and optimal control. In *Proceedings of the 19th IEEE conference on decision and control, USA* (pp. 852–864).

Bateman, A., Hull, J., & Lin, Z. (2009). A backstepping-based low and high gain design for marine vehicles. *International Journal of Robust and Nonlinear Control*, *19*, 480–493.

Fossen, T. I. (1994). *Guidance and control of ocean vehicles*. New York: John Wiley and Sons Ltd.

Fossen, T. I. (2011). *Handbook of marine craft-hydrodynamics and motion control*. New York: John Wiley and Sons Ltd.

Fossen, T. I., & Berge, S. P. (1997). Nonlinear vectorial backstepping design for global exponential tracking of marine vessels in the presence of actuator dynamics. In *Proceeding*36*th conference on decision & control*, (pp. 4237–4242), San Diego.

Fossen, T. I., & Grovlen, A. (1998). Nonlinear output feedback control of dynamically positioned ships using vectorial observer backstepping. *IEEE Transactions on Control Systems Technology*, *6*(1), 121–128.

Fossen, T. I., & Strand, J. P. (1999a). Passive nonlinear observer design for ships using Lyapunov methods: Full-scale experiments with a supply vessel. *Automatica*, *35*(1), 3–16.

Fossen, T. I., & Strand, J. P. (1999b). A tutorial on nonlinear backstepping: *Applications to ship control. Modelling, Identification and Control MIC*, *20*(June (2)), 83–135.

Fung, P. T. K., & Grimble, M. J. (1983). Dynamic ship positioning using a self-tuning Kalman filter. *IEEE Transactions on Automatic Control AC*, *28*(3), 339–350.

Grimble, M. J., Patton, R. J., & Wise, D. A. (1980). Use of Kalman filtering techniques in dynamic ship positioning. In *IEEE proceedings* (Vol. 127, pp. 93–102).

Grovlen, A., & Fossen, T. (1996). Nonlinear control of dynamic positioned ships using only position feedback: An observer backstepping approach. In *Proceedings of the 35th IEEE Conference on Decision and Control* (*CDC*'96), (pp. 3383–3393), *Kobe, Japan*.

Johansen, T. A., Fossen, T. I., & Tondel, P. (2005). Efficient optimal constrained control allocation via multi-parametric programming. *AIAA Journal of Guidence, Control and Dynamics*, *28*, 506–515.

Khalil, H. K. (2002). *Nonlinear systems*. Upper Saddle River: Prentice Hall.

Krstic, M., Kanellakopoulos, I., & Kokotovic, P. V. (1995). *Nonlinear and adaptive control design*. New York: John Wiley and Sons Inc.

Lewis, E. V. (Ed.). (1989). *Principles of naval architecture*, Vol. 3). New Jersey: The Society of Naval Architects and Marine Engineers November.

Marques, H. J. (2003). *Nonlinear control systems*. Hoboken: Wiley Interscience.

OCIMF, 1994. Prediction of wind and current loads on VCCCs. Companies International Marine Forum.

Robertsson, A., & Johansson, R. (1998). Comments on nonlinear output feedback control of dynamically positioned ships using vectorial observer backstepping. *IEEE Transaction on Control System Technology TCST*, *6*(3), 439–441.

Saelid, S., Jenssen, N. A., & Balchen, J. G. (1983). Design and analysis of a dynamic positioning system based on Kalman filtering and optimal control. *IEEE Transactions on Automatic Control AC 3*, 331–339.

Simos, A. N., Tannuri, E. A., Pesce, C. P., & Aranha, J. A. P. (2001). A quasi-explicit hydrodynamic model for the dynamic analysis of a moored fpso under current action. *Journal of Ship Research*, *45*(4), 289–301.

Sordalen, O. J. (1997). Optimal thrust allocation for marine vessels. *Control Engineering Practice*, *5*(9), 1223–1231.

Sorensen, A. J., Sagatun, S. I., & Fossen, T. I. (1996). Design of a dynamic positioning system using model based control. *Control Engineering Practice*, *4*(3), 359–368.

Sorensen, A. J., & Strand, J. P. (2000). Positioning of small-waterplane-area marine constructions with roll and pitch damping. *IFAC Journal of Control Engineering Practice CEP*, *8*(2), 205–213.

Tannuri, E. A., Agostinho, A. C., Morishita, H. M., & Moratelli, L., Jr. (2010). Dynamic positioning systems: *An experimental analysis of sliding mode control. Control Engineering Practice*, *18*(10), 1121–1132.

Tannuri, E. A., Donha, D. C., & Pesce, C. (2001). Dynamic positioning of a turred moored fpso using sliding mode control. *International Journal of Robust and Nonlinear Control 11*(13).

Tannuri, E. A., & Morishita, H. M. (2006). Experimental and numerical evaluation of a typical dynamic positioning system. *Applied Ocean Research*, *28*, 133–146.

Tannuri, E. A., & Pesce, C. P. (2002). Comparing two different control algorithms applied to dynamic positioning of a pipeline launching barge. In 10*th Mediterranean Conference on Control and Automation*, Lisbon.

Zakartchouk, A., Jr., & Morishita, H. M. (2009). Backstepping controller for dynamic positioning of ships: Simulation and experimental results for a shuttle tanker model. In *Proceedings of* 8*th IFAC conference on maneuvering and control of marine crafts* (*MCMC*2009), *Guarujá, Brazil*.